A multi-scale analysis of composite structures: application to the design of accelerated hygrothermal cycles

Z. Youssef, Frédéric Jacquemin, David Gloaguen, Ronald Guillen

A multi-scale analysis of composite structures: Application to the design of accelerated hygrothermal cycles

Z. Youssef, F. Jacquemin, D. Gloaguen, R. Guillén

GeM, Institut de Recherche en Génie Civil et Mécanique, UMR CNRS 6183, Université de Nantes – Ecole Centrale de Nantes, 37 Boulevard de l'Université, BP 406, 44602 Saint-Nazaire, France

Hygrothermal cycles are known to cause degradation of fiber-reinforced polymer composite materials due to moisture uptake and thermal expansion. The knowledge of internal stresses due to cyclic environmental conditions is necessary to forecast a possible damage occurrence in the material during its service life. The accelerated cycles are studied so as to define the material geometry and environmental conditions to reproduce the in-service material state in a shorter time. In the present work, a self-consistent (SC) model is used in order to predict the stress state at the microscopic scale (fiber and matrix) induced by the real and accelerated cycles. The main aim is to compare the local states induced by the real and accelerated cycles in particular near to the edges where hold periodic conditions.

Keywords: Moisture concentration; Hygrothermal stresses; Accelerated cycles; Self-consistent model

1. Introduction

Fiber reinforced composite laminates are increasingly used in aerospace and other engineering applications due to their light weight, high specific strength and stiffness, excellent fatigue and corrosion resistance properties. In the aeronautical applications, fiber reinforced epoxy matrix composites are exposed to severe hygrothermal and cyclical environments. When composite materials are exposed to humid environments, the moisture absorption may induce severe mechanical and physicochemical changes in polymer matrix [1] or fiber/matrix interphase [2]. In service, fiber reinforced composites are usually subjected to time-varying moisture concentration gradients producing internal hygrothermal stress which must be regarded with attention to explain material damage phenomena [3]. In particular, for composite specimens submitted to cyclical environmental conditions (aeronautical applications for instance) with temperature/moisture ageing cycles, important time-dependent gradients of internal stresses appear close to the surfaces [4]. Such gradients acting as an hygrothermal fatigue over narrow areas near to the surfaces may create some damages to the structure. Reynolds and Mc Manus [5] have shown that the effect of combination of moisture cycling and thermal cycling environments could create damage, such as cracking of material near exposed surfaces and edges.

Composite materials need to be tested to characterize and model their long-term response to hygrothermal cycles. So, the question of the design of accelerated hygrothermal cycles to meet the in-service material state in short time is addressed.

Jedidi et al. [6] have designed accelerated hygrothermal cycles to approach the long-term durability of plate composite structures subjected to supersonic flight cycles. The accelerated cycles have been conceived in such way that same average moisture concentrations as those generated by the in-service conditions are obtained. The average values of internal stresses (calculated by using the classical lamination plate theory) for the real and accelerated cycles are quite similar but it is clear that the hygrothermal fatigue of the material is different for these two kinds of cycles.

In this paper, the internal stresses due to hygrothermal cycles and near the edges are studied with attention. An accelerated cycle is designed to reproduce the moisture concentration distributions induced by a real cycle by modifying the specimen geometry and the cycle period. The macroscopic (ply) and local (fiber and matrix) internal stress states induced by the two cycles are evaluated and compared.

The moisture absorption is modelled by a Fick's law whose diffusion coefficient depends on the temperature through an Arrhénius' law. Since the temperature diffusion rate exceeds the moisture diffusion, one by several orders, it is logical to assume that the thermal equilibrium is reached instantaneously. Consequently, the thermal field inside the pipe is uniform. The moisture concentration, induced by such cyclic conditions, undergoes two patterns: a transient pattern within the pipe and a fluctuating one close to the inner and outer surfaces subjected to the periodic boundary conditions. Based on a self-consistent (SC) approach, the homogenized hygrothermoelastic (thermal and hygroscopic expansions and stiffness) properties are deduced from the properties of the fiber and matrix [7]. The hygrothermal stresses for every ply, at any time, are calculated by using the classical equations of solid mechanics: hygrothermoelastic orthotropic constitutive equations, strain–displacement relationship, compatibility and equilibrium equations and boundary conditions. Scale transition models are required to study the internal stresses in the fiber and matrix of ply [8,9]. Accelerated hygrothermal cycles representative of the real cycles are also designed. These cycles induce similar concentration and stress profiles than the real one except in regions close to the surfaces where strong gradients take place. The multi-scale analysis allows to measure the effect of discrepancies observed at the ply-scale on the induced local stresses. This question is very important because the accelerated cycle, in order to be representative, must not initiate a damage which would not be induced by the real cycle.

2. A multi-scale analysis

2.1. Identification of the homogenized thermal and hygroscopic expansion coefficients

SC models based on the mathematical formalism proposed by Kröner and Eshelby [10,11] are improved in order to take into account stresses and strains due to moisture and temperature in carbon fiber-reinforced polymer matrix composites. The material is investigated at two different scales for the needs of micromechanical modelling: the average behaviour of a ply defines the macroscopic scale, denoted by the superscript I. The properties and mechanical states of the matrix and fiber are respectively indicated by the superscripts m and f. These constituents define the microscopic (or local) scale of the material.

The hygrothermoelastic orthotropic behaviour can be written as

$$\sigma^{\alpha} = L^{\alpha} : (\varepsilon^{\alpha} - \alpha^{\alpha}\Delta T^{\alpha} - \beta^{\alpha}\Delta C^{\alpha}) \tag{1}$$

where L^{α} is the elasticity tensor of the phase α, ε the strains due to elastic and hygrothermal solicitations, α the coefficients of thermal expansion, β the coefficients of moisture expansion (CME), ΔT the temperature increment and ΔC the moisture content increment.

The macroscopic stresses and strains are the volume averages of the microscopic stresses and strains [7]:

$$\begin{aligned} \langle \sigma^{\alpha} \rangle_{\alpha=\mathrm{f,m}} &= \sigma^{\mathrm{I}} \\ \langle \varepsilon^{\alpha} \rangle_{\alpha=\mathrm{f,m}} &= \varepsilon^{\mathrm{I}} \end{aligned} \tag{2}$$

By using the Eshelby's formalism, we obtain the following relation between macroscopic and microscopic fields [8]:

$$\begin{aligned} \varepsilon^{\mathrm{I}} = {} & \langle (L^{\alpha} + L^{\mathrm{I}} : R^{\mathrm{I}})^{-1} : (L^{\mathrm{I}} + L^{\mathrm{I}} : R^{\mathrm{I}}) \rangle_{\alpha=\mathrm{f,m}} \\ & : \varepsilon^{\mathrm{I}} + \langle (L^{\alpha} + L^{\mathrm{I}} : R^{\mathrm{I}})^{-1} : [L^{\alpha} : \alpha^{\alpha}\Delta T^{\alpha} - L^{\mathrm{I}} \\ & : \alpha^{\mathrm{I}}\Delta T^{\mathrm{I}} + L^{\alpha} : \beta^{\alpha}\Delta C^{\alpha} - L^{\mathrm{I}} : \beta^{\mathrm{I}}\Delta C^{\mathrm{I}}] \rangle_{\alpha=\mathrm{f,m}} \end{aligned} \tag{3}$$

where R^{I} represents the reaction tensor that expresses the elastic interactions due to the morphology assumed for the elementary constituents of the composite material. This relation must be satisfied for any hygrothermomechanical state, so the first term of its right member must be equal to I, while the second term must be null:

$$\langle (L^{\alpha} + L^{\mathrm{I}} : R^{\mathrm{I}})^{-1} : (L^{\mathrm{I}} + L^{\mathrm{I}} : R^{\mathrm{I}}) \rangle_{\alpha=\mathrm{f,m}} = I \tag{4}$$

$$\begin{aligned} & \langle (L^{\alpha} + L^{\mathrm{I}} : R^{\mathrm{I}})^{-1} : [L^{\alpha} : \alpha^{\alpha}\Delta T^{\alpha} - L^{\mathrm{I}} : \alpha^{\mathrm{I}}\Delta T^{\mathrm{I}} + L^{\alpha} : \beta^{\alpha}\Delta C^{\alpha} \\ & \quad - L^{\mathrm{I}} : \beta^{\mathrm{I}}\Delta C^{\mathrm{I}}] \rangle_{\alpha=\mathrm{f,m}} = 0 \end{aligned} \tag{5}$$

Eq. (4) yields the very classical self-consistent estimate for the macroscopic elastic stiffness:

$$L^{\mathrm{I}} = \langle (L^{\alpha} + L^{\mathrm{I}} : R^{\mathrm{I}})^{-1} : (L^{\mathrm{I}} + L^{\mathrm{I}} : R^{\mathrm{I}}) : L^{\alpha} \rangle_{\alpha=\mathrm{f,m}} \tag{6}$$

One should notice that ΔT is considered as homogeneous at every scale. Replacing ΔC^{I} and ΔC^{α} by zero in (5), the following expression for the macroscopic thermal expansion coefficients is obtained:

$$\begin{aligned} \alpha^{\mathrm{I}} = {} & L^{\mathrm{I}^{-1}} \langle (L^{\alpha} + L^{\mathrm{I}} : R^{\mathrm{I}})^{-1} \rangle^{-1}_{\alpha=\mathrm{f,m}} : \langle (L^{\alpha} + L^{\mathrm{I}} : R^{\mathrm{I}})^{-1} : L^{\alpha} \\ & : \alpha^{\alpha} \rangle_{\alpha=\mathrm{f,m}} \end{aligned} \tag{7}$$

By assuming that the fibers do not absorb any moisture (i.e. $\Delta C^{\mathrm{f}} = 0$) and considering $\Delta T = 0$, the hygroscopic expansion coefficient β^{I} is determined through (5):

$$\begin{aligned} \beta^{\mathrm{I}} = {} & v^{\mathrm{m}} \frac{\Delta C^{\mathrm{m}}}{\Delta C^{\mathrm{I}}} L^{\mathrm{I}^{-1}} \langle (L^{\alpha} + L^{\mathrm{I}} : R^{\mathrm{I}})^{-1} \rangle^{-1}_{\alpha=\mathrm{f,m}} : (L^{\mathrm{m}} + L^{\mathrm{I}} \\ & : R^{\mathrm{I}})^{-1} : L^{\mathrm{m}} : \beta^{\mathrm{m}} \end{aligned} \tag{8}$$

where v^{m} stands for the volume fraction of the matrix in the considered ply.

When the moisture equilibrium state is reached, the moisture contents for the ply ΔC^{I} and for the neat resin ΔC^{m} are linked by Eq. (9) [12]:

$$\frac{\Delta C^{\mathrm{m}}}{\Delta C^{\mathrm{I}}} = \frac{\rho^{\mathrm{I}}}{v^{\mathrm{m}} \rho^{\mathrm{m}}} \tag{9}$$

where ρ^{I} and ρ^{m} are respectively the composite and resin densities. Introducing (9) in (8), the macroscopic CME are then expressed [9]:

$$\beta^{\mathrm{I}} = \frac{\rho^{\mathrm{I}}}{\rho^{\mathrm{m}}} L^{\mathrm{I}-1} \langle (L^{\alpha} + L^{\mathrm{I}} : R^{\mathrm{I}})^{-1} \rangle^{-1}_{\alpha=\mathrm{f},\mathrm{m}} : (L^{\mathrm{m}} + L^{\mathrm{I}} : R^{\mathrm{I}})^{-1} : L^{\mathrm{m}} : \beta^{\mathrm{m}} \tag{10}$$

The next step for a complete mechanical description at the microscopic scale is the determination of the constitutive relation which links the overall and the local stress states.

2.2. Local stress states

By assuming that the fibers do not absorb any moisture, the local stresses–strains relation (1) becomes:

$$\sigma^{\mathrm{f}} = L^{\mathrm{f}} : (\varepsilon^{\mathrm{f}} - \alpha^{\mathrm{f}} \Delta T^{\mathrm{f}}) \tag{11}$$

Using the Eshelby's formalism, one obtains, after algebraic calculations, the following scale transition expression for the strains in the fibers:

$$\varepsilon^{\mathrm{f}} = (L^{\mathrm{f}} + L^{\mathrm{I}} : R^{\mathrm{I}})^{-1} : (\sigma^{\mathrm{I}} + L^{\mathrm{f}} : \alpha^{\mathrm{f}} \Delta T^{\mathrm{f}} + L^{\mathrm{I}} : R^{\mathrm{I}} : \varepsilon^{\mathrm{I}}) \tag{12}$$

The local mechanical states in the epoxy matrix are provided by Hill's strains and stresses average laws (2):

$$\varepsilon^{\mathrm{m}} = \frac{1}{v^{\mathrm{m}}} \varepsilon^{\mathrm{I}} - \frac{v^{\mathrm{f}}}{v^{\mathrm{m}}} \varepsilon^{\mathrm{f}} \tag{13}$$

Forms (11)–(13) depend on neither the hygroscopic expansion coefficient of the matrix nor its moisture content.

3. Macroscopic hygrothermomechanical problem

To determine the local stresses, it is necessary to calculate the macroscopic hygrothermal stresses by using the effective macroscopic properties already known. We consider a thin uni-directionally reinforced composite pipe, whose inner and outer radii are a and b respectively, submitted to temperature and relative humidity cycles with the same period τ. The macroscopic moisture concentration, $c^{\mathrm{I}}(r,t)$, is solution of the following system with Fick's equation (14) whose diffusion coefficient depends on the temperature through an Arrhénius' law:

$$\frac{\partial c^{\mathrm{I}}}{\partial t} = D^{\mathrm{I}}(t) \left[\frac{\partial^2 c^{\mathrm{I}}}{\partial r^2} + \frac{1}{r} \frac{\partial c^{\mathrm{I}}}{\partial r} \right], \quad a < r < b \tag{14}$$

$$\begin{cases} c^{\mathrm{I}}(a,t) = c^{\mathrm{I}}(b,t) = c_0(t) \\ c^{\mathrm{I}}(r,0) = 0 \end{cases} \tag{15}$$

where $c_0(t)$ is the τ period boundary concentration. Because the temperature diffusion rate exceeds the moisture diffusion, one by several orders, it is logical to assume that the thermal equilibrium is reached instantaneously. Therefore, the temperature field and the diffusion coefficient through the thickness of the pipe are uniform.

The moisture concentration, induced by such cyclic conditions, undergoes two patterns: a transient then permanent pattern in the internal regions of the composite structure and a fluctuating then periodic pattern in regions close to the lateral surfaces. The extent of the fluctuating part e_0 is approximated by the following expression [13]:

$$e_0 = 2\sqrt{\pi \int_0^{\tau} D^{\mathrm{I}}(t)\,\mathrm{d}t} \tag{16}$$

The hygrothermoelastic orthotropic behaviour is given by Eq. (1). To solve the hygrothermomechanical problem, it is necessary to express the strains versus the displacements along with the compatibility and equilibrium equations [4].

Displacements with respect to the longitudinal direction x and ortho-radial direction θ, respectively $u^{\mathrm{I}}(x,r)$ and $v^{\mathrm{I}}(x,r)$ are then deduced [4]:

$$\begin{cases} u^{\mathrm{I}}(x,r) = R_1 x \\ v^{\mathrm{I}}(x,r) = R_2 x r \\ R_1, R_2 \text{ are constants} \end{cases} \tag{17}$$

It is worth noticing that the displacements $u^{\mathrm{I}}(x,r)$ and $v^{\mathrm{I}}(x,r)$ do not depend at all upon the hygrothermal field. The fluctuating concentration is determined by using a finite difference scheme [4]. In order to propose a closed form solution of the displacement component in the radial direction, the regions close to the two lateral surfaces, where hold fluctuating concentrations, are subdivided and on each subdivision a parabolic moisture concentration distribution is assumed:

$$c_i^{\mathrm{I}} = A_i r^2 + B_i r + C_i \tag{18}$$

A_i, B_i, C_i are constant.

Finally, we obtain the radial component of the displacement field for each subdivision:

$$\begin{aligned} w^{\mathrm{I}}(r) = {} & R_3 r \sqrt{\frac{L^{\mathrm{I}}_{\theta\theta}}{L^{\mathrm{I}}_{rr}}} + R_4 r \sqrt{\frac{L^{\mathrm{I}}_{\theta\theta}}{L^{\mathrm{I}}_{rr}}} + \frac{(L^{\mathrm{I}}_{x\theta} - L^{\mathrm{I}}_{xr}) R_1 r}{L^{\mathrm{I}}_{rr}\left(1 - \frac{L^{\mathrm{I}}_{\theta\theta}}{L^{\mathrm{I}}_{rr}}\right)} \\ & + \frac{(I_1 - I_2)(T - T_0) r}{L^{\mathrm{I}}_{rr}\left(1 - \frac{L^{\mathrm{I}}_{\theta\theta}}{L^{\mathrm{I}}_{rr}}\right)} + \frac{(L^{\mathrm{I}}_{s\theta} - 2L^{\mathrm{I}}_{rs}) R_2 r^2}{L^{\mathrm{I}}_{rr}\left(4 - \frac{L^{\mathrm{I}}_{\theta\theta}}{L^{\mathrm{I}}_{rr}}\right)} \\ & + \frac{(K_1 - K_2)}{\rho^{\mathrm{I}} L^{\mathrm{I}}_{rr}} \left[\frac{C_i r}{\left(1 - \frac{L^{\mathrm{I}}_{\theta\theta}}{L^{\mathrm{I}}_{rr}}\right)} + \frac{B_i r^2}{\left(4 - \frac{L^{\mathrm{I}}_{\theta\theta}}{L^{\mathrm{I}}_{rr}}\right)} + \frac{A_i r^3}{\left(9 - \frac{L^{\mathrm{I}}_{\theta\theta}}{L^{\mathrm{I}}_{rr}}\right)} \right] \\ & + \frac{K_1}{\rho^{\mathrm{I}} L^{\mathrm{I}}_{rr}} \left[\frac{B_i r^2}{\left(4 - \frac{L^{\mathrm{I}}_{\theta\theta}}{L^{\mathrm{I}}_{rr}}\right)} + \frac{2A_i r^3}{\left(9 - \frac{L^{\mathrm{I}}_{\theta\theta}}{L^{\mathrm{I}}_{rr}}\right)} \right] \end{aligned} \tag{19}$$

with

$$\begin{aligned} I_1 &= L^{\mathrm{I}}_{xr}\alpha^{\mathrm{I}}_{xx} + L^{\mathrm{I}}_{r\theta}\alpha^{\mathrm{I}}_{\theta\theta} + L^{\mathrm{I}}_{rr}\alpha^{\mathrm{I}}_{rr} + L^{\mathrm{I}}_{rs}\alpha^{\mathrm{I}}_{x\theta}, \\ I_2 &= L^{\mathrm{I}}_{x\theta}\alpha^{\mathrm{I}}_{xx} + L^{\mathrm{I}}_{\theta\theta}\alpha^{\mathrm{I}}_{\theta\theta} + L^{\mathrm{I}}_{r\theta}\alpha^{\mathrm{I}}_{rr} + L^{\mathrm{I}}_{s\theta}\alpha^{\mathrm{I}}_{x\theta}, \\ K_1 &= L^{\mathrm{I}}_{xr}\beta^{\mathrm{I}}_{xx} + L^{\mathrm{I}}_{r\theta}\beta^{\mathrm{I}}_{\theta\theta} + L^{\mathrm{I}}_{rr}\beta^{\mathrm{I}}_{rr} + L^{\mathrm{I}}_{rs}\beta^{\mathrm{I}}_{x\theta}, \\ K_2 &= L^{\mathrm{I}}_{x\theta}\beta^{\mathrm{I}}_{xx} + L^{\mathrm{I}}_{\theta\theta}\beta^{\mathrm{I}}_{\theta\theta} + L^{\mathrm{I}}_{r\theta}\beta^{\mathrm{I}}_{rr} + L^{\mathrm{I}}_{s\theta}\beta^{\mathrm{I}}_{x\theta}. \end{aligned}$$

L^{I}, α^{I} and β^{I} are, respectively, the macroscopic elastic stiffness and the macroscopic thermal and hygroscopic

expansion coefficients calculated with Eqs. (6)–(8) based on the SC approach.

Finally, the displacement field depends on four constants to be determined: R_i for $i = 1, \ldots, 4$. These four constants are deduced from the following conditions:

- global force balance of the cylinder,
- nullity of the normal stress on the two lateral surfaces.

4. Example

Complementary models presented in Sections 2 and 3 have been used to determine the macroscopic properties and the mechanical stresses at two different scales in each ply of a composite structure subjected to cyclical temperature and relative humidity. The macroscopic model also ensures the calculation of the macroscopic moisture content.

Let us consider a thin ±55 angle-ply pipe made up of eight orthotropic unidirectional T300/5208 carbon fiber/epoxy plies of equal thickness. The thickness of the pipe is 4 mm and the fiber volume fraction is 60%. The mechanical and hygrothermal properties of the carbon fiber and epoxy matrix are summarised in Tables 1 and 2 [8,14,15].

Fig. 1 shows the experimental temperature and relative humidity cycles used as reference in order to define an accelerated representative cycle [5].

Five particular points have been chosen on the cycle in order to represent the concentration and stress evolutions during the cycle. These points have been selected because they characterise important changes of the relative humidity or temperature.

These cycles include: cold/dry (−54 °C) for 10 min, hot/dry (163 °C) for 30 min, warm/wet (87 °C, 85% H) for 60 min, heating rate 11 °C/min, cooling rate 5.5 °C/min, 160 min/cycle.

Table 1
Mechanical properties of T300/5208 constituents

Material	E_1 (GPa)	E_2, E_3 (GPa)	υ_{12}, υ_{13}	G_{23} (GPa)	G_{12} (GPa)
T300	230	15	0.2	7	15
N5208	2.9	2.9	0.35	1.07	1.07

Table 2
Hygrothermal properties of T300/5208 constituents

Material	α_1 (K^{-1})	α_2 (K^{-1})	β_1	β_2
T300	-0.7×10^{-6}	12×10^{-6}	0	0
N5208	60×10^{-6}	60×10^{-6}	0.6	0.6

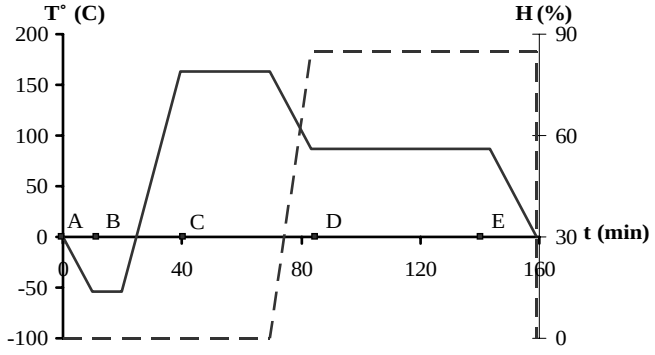

Fig. 1. Temperature and relative humidity cycles [5].

4.1. Calculation of moisture concentration profiles

The diffusion coefficient D^{I} and the boundary moisture concentration c_0 are indicated in Table 3.

The finite differences method is used to solve the set of diffusion equations (14) and (15) and calculate the concentration profiles, inside the pipe, induced by the hygrothermal cycles.

The moisture concentration evolution, function of number of cycles, is represented in Fig. 2. This evolution is estimated at point E where simultaneous changes of temperature and relative humidity appear. The extent e_0 of the periodic concentration during permanent state is presented in Fig. 3.

Table 3
Hygroscopic properties of T300/5208 [12]

Material	D^{I} (mm^2/s)	Moisture concentration c_0 (kg/m^3)
T300/5208	$0.57\exp(-4993/T(t))$	0.2385 H

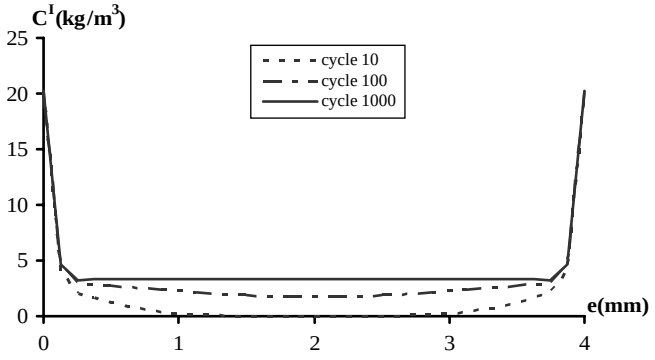

Fig. 2. T300/5208 concentration profiles.

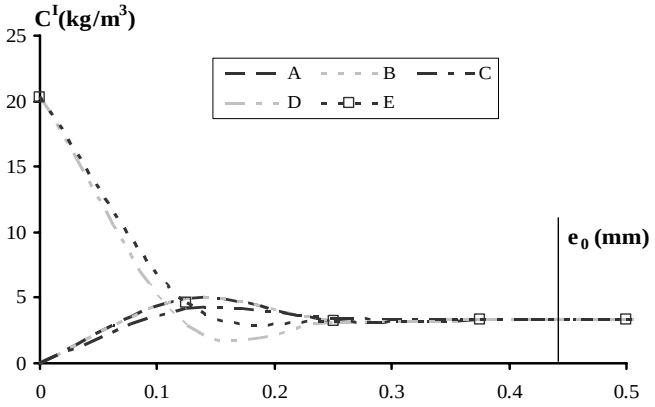

Fig. 3. Extent e_0 of the periodic concentration.

The numerical simulations reveal that the moisture concentration, induced by such cyclic conditions, undergoes two patterns: a transient pattern, within the pipe, which tends towards a permanent solution after 1000 cycles (Fig. 2) and a fluctuating (then periodic when the permanent state is reached inside the pipe) pattern close to the inner and outer surfaces subjected to the periodic boundary conditions. The extent e_0 of the fluctuating then periodic moisture concentration is about 0.45 mm (Fig. 3).

4.2. Design of accelerated hygrothermal cycles

The question addressed here is to design accelerated hygrothermal cycles to reproduce the real moisture concentration profiles and thus the induced mechanical states. A particular attention will be pointed out on the regions close to the surfaces where strong moisture gradients take place. Firstly, the objective is to reproduce these moisture concentration profiles in a shorter time by modifying the thickness of the specimen and reducing the period of the hygrothermal cycles.

The thickness e of the pipe was reduced to 2 mm and the period of the hygrothermal cycles was also shortened to define the accelerated cycles. The value of the period is analytically calculated using Eq. (14) in order to keep the same proportionality e_0/e compared to the real cycles.

These accelerated environments included: cold/dry (−54 °C) for 2.5 min, hot/dry (163 °C) for 7.5 min, warm/wet (87 °C, 85% H) for 14 min, heating rate 44 °C/min, cooling rate 22 °C/min, 40 min/cycle (Fig. 4).

Fig. 5 shows that the extent e_0 of the periodic concentration induced by such accelerated cycles is 0.225 mm.

Fig. 6 presents the moisture concentration induced by the real and accelerated cycles during transient and permanent states as a function of a normalised radial distance.

The comparison is carried out at point E corresponding to a brutal evolution of the moisture concentration at the edge.

The evolutions of the transient and permanent concentration inside the pipe due to the real and accelerated cycles are in perfect correlation. The transient pattern tends towards a permanent solution after 1000 accelerated cycles: conditioning time associated to the accelerated cycle is four

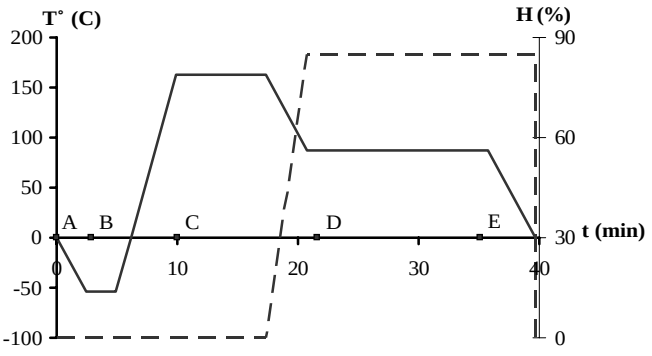

Fig. 4. Accelerated hygrothermal cycles.

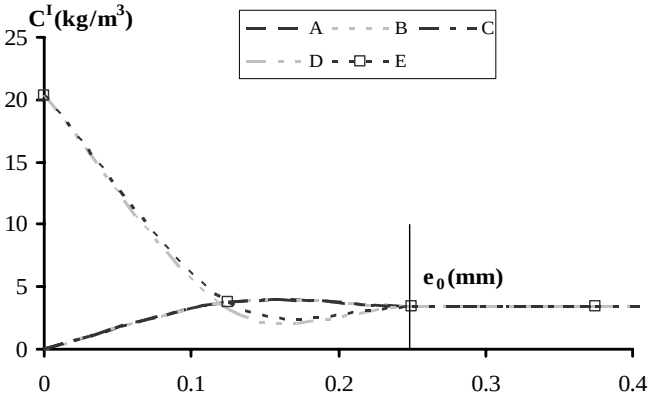

Fig. 5. Extent e_0 of the periodic concentration for the accelerated cycles.

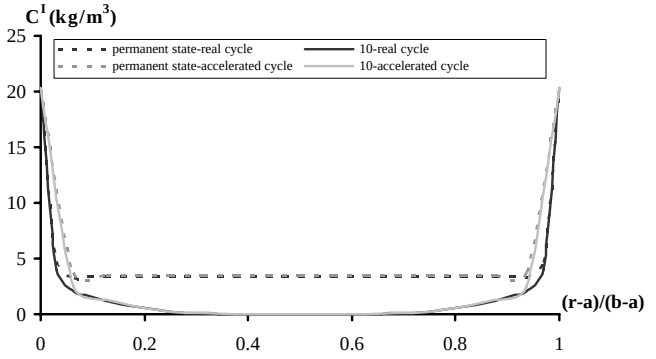

Fig. 6. Comparison of the concentrations induced by the real and accelerated cycles at point E.

times faster than the real one. The light difference of moisture concentrations between the two cycles appears in the vicinity of the external surfaces where the fluctuating then periodic concentrations (Fig. 7) reign.

4.3. Mechanical calculation

4.3.1. Estimation of the effective properties

The macroscopic elastic stiffness has been calculated, using the self-consistent approach (6), by assuming the following values for the length of the semi-axis of the inclu-

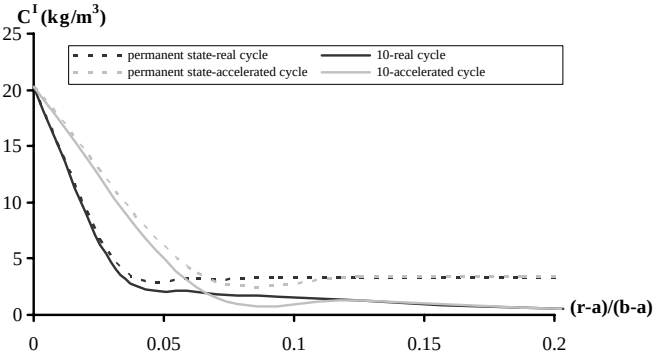

Fig. 7. Concentrations at the edge induced by the real and accelerated cycles.

sions, in order to take into account the fiber microstructure of the material: $a_2 = a_3 = 1$ and $a_1 = 100$.

a_1, a_2 and a_3 are respectively the longitudinal, transverse and normal semi-axis of the ellipsoidal inclusion. The homogenised mechanical properties calculated by using the SC model are represented in Table 4.

The calculation of the macroscopic CME is carried out for a ratio $\Delta C^{m}/\Delta C^{I} = 3.33$ corresponding to zero void fraction and perfect adhesion between fiber and matrix [9]. The homogenized coefficients of moisture and thermal expansions estimated through the SC model are presented in Table 5.

4.3.2. Macroscopic stress states

Knowing the macroscopic effective properties and using Eq. (1), the macroscopic stresses can be calculated. The macroscopic transverse and shear stresses, induced by the real and accelerated cycles for transient and permanent states, are plotted in Figs. 8 and 9.

The increase of the temperature at point E to 87 °C, creates compressive transverse stresses in the pipe. These stresses grow with the concentration of moisture and the number of cycles. They reach a constant value within the pipe during the permanent state. Fig. 8 shows that the transverse stresses σ_{22} are sensitive to the cyclical concentration gradients close to the boundaries, where the fluctuating then periodic solutions prevail. In these regions, strong stress gradients hold and a maximum value of 110 MPa is attained.

Contrary to the evolution of σ_{22}, the shear stresses do not depend on the fluctuating solutions. These stresses

Table 4
Mechanical properties of T300/5208 composite

Material	E_1 (GPa)	E_2 (GPa)	ν_{12}, ν_{13}	G_{23} (GPa)	G_{12} (GPa)
T300/5208	138.7	7.75	0.25	2.94	5.68

Table 5
Predicted hygrothermal properties of T300/5208 composite

Material	α_1^I (K^{-1})	α_2^I (K^{-1})	β_1^I	β_2^I
T300/5208	-0.06×10^{-6}	34.77×10^{-6}	0.02	0.88

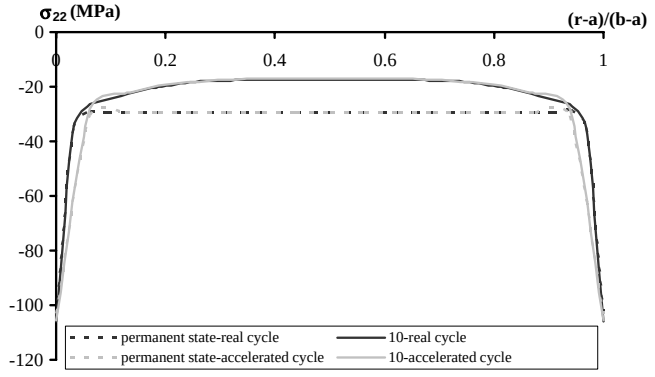

Fig. 8. Macroscopic transverse stresses at point E.

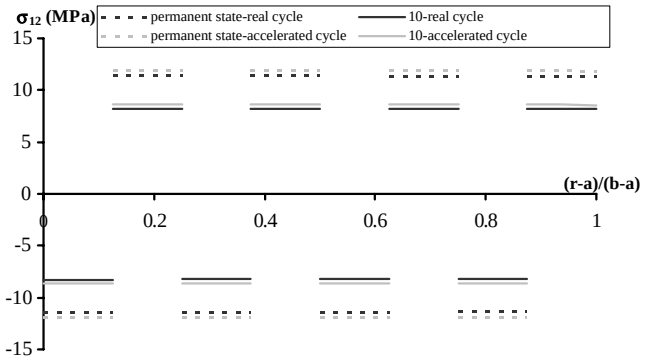

Fig. 9. Macroscopic shear stresses at point E.

are constant within the pipe during the transient and permanent state. The discontinuity of the shear stresses is only due to the stacking sequence.

On Figs. 8 and 9, similar shear and transverse stress profiles for the real and accelerated cycles are observed. The difference between the profiles of the transverse stresses for the two cycles appears in regions close to the surfaces where strong gradients take place (Fig. 8). Thus, it is necessary to study if this difference causes important discrepancies on the level of the corresponding local stresses.

4.3.3. Local stress states

4.3.3.1. Local stress states in the central ply. The local stresses are deduced from the macroscopic stresses by using the equations of the SC model (see Section 2). Figs. 10 and 11 represent the comparison between the transverse and shear stresses for the real and accelerated cycles when permanent patterns are reached. The evolution of the macroscopic and local stresses is determined for the particular points chosen during the hygrothermal cycle.

The transverse stresses in the central ply and in the constitutive matrix and fibers are compressive during the permanent pattern and attain maximum values at point C where the temperature increases to 163 °C. The thermal effect for the fibers is dominant because they do not absorb any moisture. The matrix undergoes the highest transverse stresses.

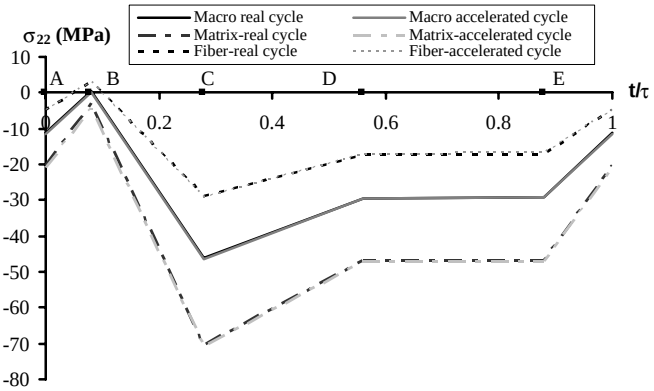

Fig. 10. Transverse stresses in the central ply during the permanent pattern.

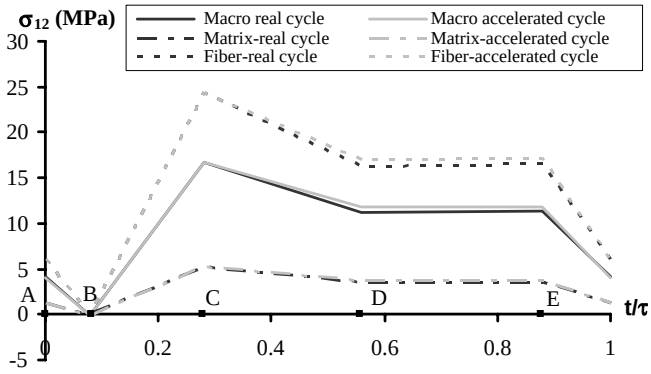

Fig. 11. Shear stresses in the central ply during the permanent pattern.

At the macroscopic and microscopic levels, tensile shear stresses are observed. the temperature change from 0 °C to −54 °C, at point *B*, produces null shear stresses. A good correlation between the macroscopic and local stresses, for the central ply, induced by the real and accelerated cycles, is obtained. The numerical results show clearly the contrast between internal stresses within fiber and matrix. The present model can describe with accuracy the development of stress heterogeneities during hygrothermal cycles.

4.3.3.2. Local stress states in the ply at the edge. The aim of this section is the comparison between the local mechanical states induced by the real and accelerated cycles for the external ply where holds fluctuating concentrations. Fig. 12 shows that the magnitude of the transverse stress in the external ply depends on the combined variations of the temperature and moisture. the decrease of temperature at point *B* to −54 °C, induces a tensile value around 7 MPa whereas the increase of temperature at point *C* to 163 °C, involves a compressive value around −65 MPa in the matrix. At point *D*, a relative humidity of 85% and a temperature of 87 °C involve a compressive value around −110 MPa for the transverse stress in the matrix.

Weak differences between macroscopic and microscopic transverse stresses induced by the real and accelerated cycles, for the ply at the edge, are observed during the permanent pattern.

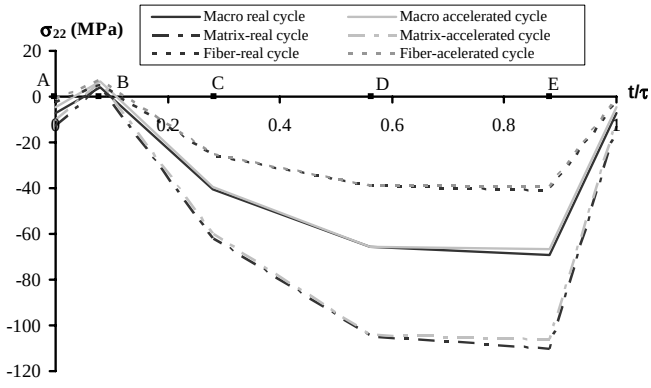

Fig. 12. Transverse stresses in the ply at the edge during the permanent pattern.

The decrease of the temperature at point *B* to −54 °C induces null shear stresses for the external ply (Fig. 13). The shear stresses in the ply, matrix and fiber remain negative in the permanent pattern and reach maximum values at point *C* where the temperature increases to 163 °C. the shear stresses, present in permanent pattern, are far away from the ply macroscopic resistance (68 MPa [15]).

The comparison of the stresses in the external ply during the 10th cycle, induced by the two cycles, are plotted in Figs. 14 and 15.

The transverse stresses for the external ply, plotted in Fig. 14, during the 10th cycle are quasi-identical as the permanent transverse stresses. Close to the surfaces, the strong moisture concentration gradients, present in the first times, play a significant role on the induced stresses.

In the matrix, the difference between the transverse stresses induced by the two cycles is more pronounced compared to the permanent state. For the first cycles, the moisture concentration is quasi-null inside the pipe while strong gradients (difficult to reproduce) subsist near to the edges. The more pronounced difference observed for the macroscopic fields has an influence on the induced microscopic fields. For instance, in the matrix at point *E*, the real transverse stress is equal to −110 MPa and the accelerated transverse stress is equal to −104 MPa. Nevertheless, at the microscopic

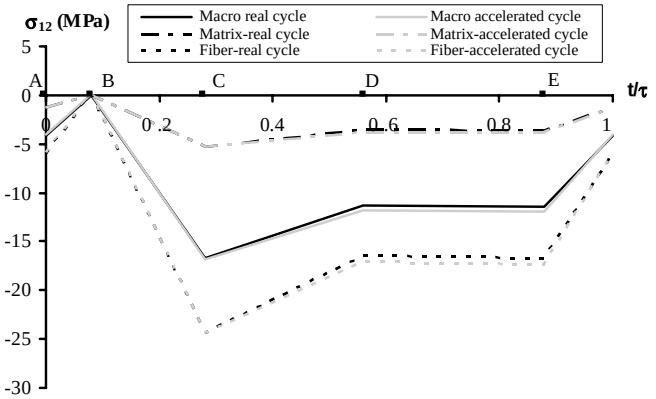

Fig. 13. Shear stresses in the ply at the edge during the permanent pattern.

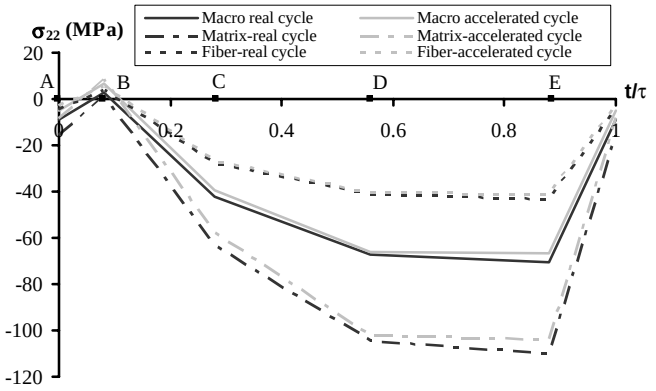

Fig. 14. Transverse stresses in the ply at the edge during the cycle 10.

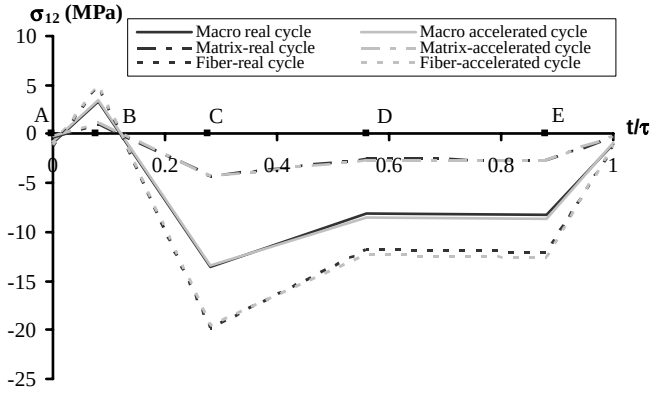

Fig. 15. Shear stresses in the ply at the edge during cycle 10.

and macroscopic scales, the accelerated hygrothermal cycle induces transverse stresses close to the real ones for both the transient and permanent patterns.

The maximum values (matrix and macro) of the shear stress at point *C* are lower compared to the permanent pattern values. This phenomenon is caused by the reduction of the ply and matrix moisture contents. Then, the cooling process at point *B* creates shear stresses in the fiber close to 5 MPa.

5. Conclusions

Evolutions of internal stresses due to hygrothermal cycles within fiber reinforced composites have been analyzed using a multi-scale approach. The macroscopic stresses are calculated by using the continuum mechanism formalism and the local stresses are deduced from the self-consistent scale transition model. The accelerated hygrothermal cycles representative of the real ones are also designed so as to define the material geometry and environmental conditions to reproduce the in-service material state in shorter time. The period of the hygrothermal cycles and the material thickness are reduced to define the accelerated cycle. Such cycles induce similar concentration and stress profiles compared to the real ones except in regions close to the surfaces where strong gradients take place. The multi-scale approach shows that the discrepancies observed at the ply-scale in these regions do not involve strong differences on the induced local stresses. This kind of approach allows assessment of the relevance of accelerated cycles in a more effective way, based on determination of the mechanical state at different levels of the material.

References

[1] Didierjean S, Michel L, Barrau JJ, Paroissien E. Predicting the behaviour of graphite/epoxy laminates under hydrothermal loads. In: Proceedings of euromech 453 conference internal stresses in polymer composite processing and service life, Saint-Etienne, 1–3 December 2003.

[2] Weitsman Y. Moisture in composites: sorption and damage. Fatig Compos Mater 1990;9:385–429.

[3] Weitsman YJ. Anomalous fluid sorption in polymeric composites and its relation to fluid-induced damage. Compos Part A: Appl Sci Manufact 2005:1–7.

[4] Jacquemin F, Vautrin A. A closed-form solution for the internal stresses in thick composite cylinders induced by cyclical environmental conditions. Compos Struct 2002;58:1–9.

[5] Reynolds TG, Mc Manus HL. Accelerated tests of environmental degradation in composite materials. In: Grant P, Rousseau CQ, editors. Composite structures: theory and practice. ASTM STP 1383. West Conshohocken, PA: American Society for Testing and Materials; 2000. p. 513–25.

[6] Jedidi J, Jacquemin F, Vautrin A. Design of accelerated hygrothermal cycles on polymer matrix composites in the case of a supersonic aircraft. Compos Struct 2004;68:429–37.

[7] Hill R. The essential structure of constitutive laws for metals composites and polycrystals. J Mech Phys Solids 1967;15:79–95.

[8] Jacquemin F, Fréour S, Guillén R. A hygro-elastic self-consistent model for fiber-reinforced composites. J Reinf Plast Compos 2004;5:485–502.

[9] Fréour S, Jacquemin F, Guillén R. On an analytical self-consistent model for internal stress prediction in fiber-reinforced composites submitted to hygroelastic load. J Reinf Plast Compos 2005;24:1365–77.

[10] Eshelby JD. The determination of the elastic field of an ellipsoidal inclusion and related problems. Proc Roy Soc Lond 1957;A241:376–96.

[11] Kröner E. Berechnung der elastischen Konstanten des Vielkristalls aus des Konstanten des Einkristalls. Z Phys 1958;151:504–18.

[12] Loos AC, Springer GS. Environmental effects on composite materials, moisture absorption of graphite–epoxy composition immersed in liquids and in humid air. Tech Publish 1981:34–55.

[13] Verchery G. Moisture diffusion in polymeric matrix composites with cyclic environmental conditions. In: Bunsell AR, Jamet JF, Massiah A, editors. Proceedings of the 5th European conference on composite materials (ECCM5), Bordeaux, France, 1992. p. 505–10.

[14] Agbossou A, Pastor J. Thermal stresses and thermal expansion coefficients of *n*-layered fiber-reinforced composites. Compos Sci Technol 1997;57:249–60.

[15] Soden PD, Hinton MJ, Kaddour AS. Lamina properties, lay-up configurations and loading conditions for a range of fibre-reinforced composite laminates. Compos Sci Technol 1998;58:1011–22.